JVST A
Journal of Vacuum Science & Technology A

ARTICLE

avs.scitation.org/journal/jva

3D-printed and injection molded polymer matrix composites with 2D layered materials

Cite as: J. Vac. Sci. Technol. A 38, 042201 (2020); doi: 10.1116/6.0000121
Submitted: 14 February 2020 · Accepted: 4 June 2020 ·
Published Online: 26 June 2020

Gerardo Gamboa,[1] Sangram Mazumder,[1] Nathalie Hnatchuk,[1] Jorge A. Catalan,[2] Damaris Cortes,[2] IKang Chen,[1] Perla Perez,[2] Witold Brostow,[1,a)] and Anupama B. Kaul[1,3,a)]

AFFILIATIONS

[1]Department of Materials Science and Engineering; PACCAR Technology Institute, University of North Texas, Denton, Texas 76203
[2]Department of Metallurgical, Materials and Biomedical Engineering, University of Texas at El Paso, El Paso, Texas 79968
[3]Department of Electrical Engineering, University of North Texas, Denton, Texas 76203

[a)]**Authors to whom correspondence should be addressed:** anupama.kaul@unt.edu and wkbrostow@gmail.com

ABSTRACT

Two-dimensional layered materials (2DLMs), MoS_2 and WS_2, and three-dimensional (3D) graphite were infused in thermoplastic polymer matrices comprised of acrylonitrile butadiene styrene (ABS) and polyethylene terephthalate glycol (PETG). Two processing approaches were examined for creating polymer tensile test specimens using the composites for mechanical testing, which included three-dimensional (3D) printing and injection molding. The ductility generally decreased with the addition of the fillers indicated by an increase in Young's modulus and a corresponding decrease in yield stress and tensile stress for the 2DLM-polymer composites. The dynamic friction data of the composites were measured in an attempt to exploit the solid phase lubricating properties of graphite and the 2DLM fillers. Graphite proved to lower the dynamic friction in the cases of 3D printed PETG and injection molded ABS, while MoS_2 and WS_2 were found to reduce friction in 3D printed PETG and ABS. Finally, the thermal conductivities of these polymer matrix composites were measured and compared to the pure polymer matrices. The thermal conductivity increased in both ABS and PETG composites containing graphite, MoS_2, and WS_2, irrespective of their processing routes. The use of 2DLM-based polymer composites remains an area of interest for a wide range of applications in the future, such as wearable electronics and sensors with low-cost additive manufacturing approaches.

I. INTRODUCTION

The immense success of graphene, a honeycomb arrangement of carbon atoms in a planar sheet, has been followed by a spectacular rush in the research and development of other two-dimensional (2D) materials that form monolayer atomic sheets with phenomenal properties. The 2D material library is growing every year with the addition of layered materials that can effortlessly be split into subnanometer scale materials.[1–3] These materials cover 2D transition metal dichalcogenide monolayers (2D TMDs) such as molybdenum disulfide and diselenide (MoS_2 and $MoSe_2$), tungsten disulfide and diselenide (WS_2 and WSe_2), and hexagonal boron nitride (h-BN), to name a few.[4–6] The 2D TMDs demonstrate distinct electrical and optical properties believed to originate from quantum confinement leading to the indirect-to-direct bandgap transition when bulk materials are scaled down to the nanoscale, specifically, monolayers.[7] The unique tunable bandgap property of TMDs makes them a very promising material for various optoelectronic devices, which include light emitting diodes,[8] solar cells,[9] and quantum-enabled devices.[10] Along with their superior optoelectronic properties, graphite, MoS_2, as well as WS_2 have displayed exceptional tribological wear-resistant characteristics useful for solid lubrication.[11,12]

The 2D materials encompass large surface area to volume ratios given their large areal and yet ultra-thin membrane like structural attributes, which should enhance their role in composites arising from the polymer-2D material interfaces.[13] This unique property would be strengthened if the dispersion is homogeneous within the composites.[14] Hence, it is important to note that the enhancement of different properties is strictly related to homogeneous mixing of the dispersed and the matrix phases. Polymer based nanocomposites incorporated with strong and durable multifunctional nanoparticles such as fullerenes, carbon nanotubes, and graphene sheets[13–15] have been demonstrated, which improved the

mechanical properties compared to conventional composites,[15,16] corrosion and wear resistance,[17,18] thermal conductivity,[19] and electrical conductivity.[20]

In this study, 2D TMDs (MoS_2 and WS_2) and the 3D allotrope of carbon and graphite were incorporated into acrylonitrile butadiene styrene (ABS) and polyethylene terephthalate glycol (PETG) matrices in order to form polymer matrix composites (PMCs). Three-dimensional printing (3D-P) and injection molding (IM) were used as two candidate-processing routes to test various properties of the PMCs so the importance of processing route is better discerned. Apart from mechanical properties, thermal and frictional characteristics of the parent ABS and PETG matrices were also studied and compared with the added 2D TMD and graphite fillers.

The multipronged analysis described in this study was motivated by the purpose to fuse together topics of low-cost, additive manufacturing with 2D layered materials, and studying their ensuing mechanical and tribological properties. The composites are made from thermoplastic polymers, specifically PETG and ABS acting as the matrix material. The fillers used were graphite and 2D TMDs. Our aim was to explore the variation in mechanical properties with varying concentrations of graphite and TMDs added to the matrix. While there is a plethora of work exploring the electronic and optoelectronic properties of these van der Waals solids, studies on forming composites with these materials have received little attention. Given the wide reach of additive manufacturing in defense, healthcare, and the wearable electronics industry, this work is well positioned to guide future efforts to further extend the prospects of 2D layered materials in hybrid platforms with polymeric systems, where processing challenges need to be understood and overcome to enable novel applications in the future.

II. RESULTS AND DISCUSSION

A. Preparation of the 2D TMD composites and graphite polymer matrix composites using 3D-P and IM

The 3D-P and IM samples were prepared by dispersing the 2D TMDs and graphite fillers in weight percentages ranging from 0% to 20% (0, 1, 5, 10, 15, and 20%) in the matrices. Before mixing the fillers with the polymers, from our prior work on 2D layered materials dispersions (e.g., Ref. 13), we have used dynamic light scattering for estimating the aspect ratio for as prepared nanosheets as a function of sonication time. In this prior work,[13] we have computed the fragmentation rate of 2D layered materials (e.g., MoS_2, WS_2, and graphite used in this work) when these were dispersed in solvents, where the fragmentation rate is a measure of the particle size reduction with ultrasonication time. From this work, we determined that the highest fragmentation rate generally occurred for sonication times of ~30 min, and our filler materials here were sonicated for well beyond these times as well. Traditional tensile test samples were 3D-P and IM into tensile test samples (ASTM D638 Type V) for the mechanical tests. The samples were then tensile tested to find the Young's modulus, yield stress, tensile stress, and the strain percent at fracture and the results were compared to the control samples (pure ABS and PETG). The fracture surfaces were examined using scanning electron microscopy (SEM) to understand the nature of the fracture surface through the presence of stress concentrators (typically voids in the PMC), given the two processing routes. Because of their lubricating properties, the extent of lubrication attained because of infusing these 2D TMDs/graphite materials into the polymer matrix bases was also analyzed. Since these 2D TMDs are better thermal conductors compared to PETG and ABS, their incorporation into the insulating polymer should enhance base thermal conductivity, which was also studied in this work.

For the 3D-P samples, the PMC filaments were produced using a Filabot EX2 extruder and a Filabot spooler. The synthetic graphite powder had an average particle size of 500 μm, which was problematic because the printer's nozzle was 300 μm. In order to overcome this problem, the graphite powder was placed in an IPA solution and the solution was placed in a Shear Mixer at 5000 rpm for 5 min. After exfoliation, the graphite particle size was reduced to an average of ~40 μm. The resultant powder was dried at 90 C in an oven for 1 day.

The PETG pellets were also dried at 65 °C for 4 h to remove all the trapped moisture within the pellets. After drying the PETG pellets, the 2D fillers were weighed in different ratios to create the composite with the desired weight percent. For example, 1 g of graphite was mixed inside a plastic container with 99 g of PETG pellets, which resulted in a 1% graphite–PETG composite sample. To ensure the initial loadings provided the desired final concentrations, two samples of identical volume (5×1.75 mm^2) were compared, PETG pure and PETG with graphite with the load. The masses were compared and the mass difference of the PETG with graphite was taken to be the loading fraction of filler material that made it into the matrix. These calculations showed that the differences between the original and the final loading fraction are negligible. The same procedure was then used with other ratios of treated graphite powder with the PETG pellets; i.e., 5 g of graphite and 95 g of PETG pellets, 10 gm graphite and 90 gm PETG pellets, 15 gm graphite and 85 gm PETG pellets, and finally, 20 gm graphite and 80 gm PETG pellets. A second set of 5 spools was formed using ABS and the shear mixed graphite powders at concentrations of 1, 5, 10, 15, and 20% graphite to yield the graphite–ABS composite filaments. Similar process was used to fabricate filaments of PETG with MoS_2 (Alfa Aesar, 98%, LOT: P12B015) and WS_2 (Alfa Aesar, 99.8% LOT: N01C036) dispersed in the polymer. In order to extrude the PMCs, each solid mixture (filler in polymer) of pellets were fed individually into the Filabot extruder. After extrusion, one set of ABS/PETG-fillers samples were 3D-P and another set of ABS/PETG-filler samples were IM to prepare the tensile test specimens (ASTM D638 Type V).

Injection molding of the ABS/PETG fillers samples was performed using an AB Machinery (AB-100) injection molding apparatus. The filaments were cut into small pieces and were introduced into the "feed" of the IM apparatus. The contents of the feed were then pushed into the body chamber where a temperature of 250 °C for ABS PMCs and 270 °C for PETG PMCs was used, in order to completely melt the PMCs. The melt was then pushed through the nozzle into the specimen mold having dimensions identical to ASTM D638 Type V.

For 3D printing, nozzle temperature, bed temperature, and Z-offset were important parameters to consider for 3D printing the samples. Nozzle temperature was changed for the PETG composites compared to the ABS based composites given the difference in

the melt temperature. Filler materials also had an impact on the printing temperature used since their presence in large loading quantities required the nozzle temperature to be modified for optimal results. For pure ABS and PETG, nozzle temperature was set at ~245 °C and ~220 °C, respectively. The nozzle temperature had to be lowered to ~230 °C and ~215 °C with the addition of 20% graphite to both polymers. For PETG with the addition of MoS_2 and WS_2 fillers, the nozzle temperature had to be increased to ~240 °C at 20% loading. The Z–offset, which is the distance between the tip of the nozzle and the surface of the bed, also had to be monitored depending on the type of PMC printed. Interestingly, the Z-offset was kept at ~0.1 mm for ABS, but for PETG a negative Z-offset was required down to less than few mm. The path was set to the default of the Lulzbot TAZ 6 printer. Finally, the bed temperature was maintained at ~100 °C for these experiments, except for the case of WS_2 where the bed temperature was lowered further down to ~70 °C.a

B. Tensile testing results

Tensile testing of all samples was done using the ADMET MEP—130214-7 tensile testing apparatus. Figure 1(a) demonstrates the process flow for preparing the PMCs, while Fig. 1(b) depicts the prepared ASTM dog-bone tensile test samples, where the top and the bottom insets visually reveal the differences in surface morphology for 3D-P samples compared to IM, respectively, with the former being generally far rougher. Figure 2(a) shows the stress versus strain curves for pure ABS and PETG processed samples prepared with 3D-P and IM. These data revealed that the IM ABS and PETG samples are tougher compared to the 3D-P samples which fractured earlier. As can be seen in Fig. 2(a), the tensile toughness defined as the area under the tensile stress versus strain curve is very large for IM ABS and for IM PETG. The respective values for 3D-P ABS and 3D-P PETG are much smaller. Thus, we have here an important factor for choosing one of the processing routes. The stress-strain plots for the composite materials are shown in Figs. S1 and S2 (supplementary material).[25]

The yield stress for the PMCs is plotted in Figs. 2(b) and 2(c) for IM (b) and 3D-P (c) samples as a function of filler concentration, while Young's Modulus is shown in Fig. 2(d) for IM and Fig. 2(e) for 3D-P samples. The yield stress of pure PETG was generally larger than that of pure ABS for either processing route by about 2.7 MPa in IM (53.67 versus 50.94 MPa, respectively) and about 7.1 MPa in 3D-P (49.16 versus 42.05 MPa). Young's modulus showed an opposite trend for the pure plastics. For the ABS samples, Young's modulus was larger than PETG by about 220 MPa in 3D-P (1820 versus 1600 MPa) and about 340 MPa in IM (1245 versus 340 MPa). For IM samples in Fig. 2(b), the addition of 1% graphite decreased yield stress of the composites by about 15 MPa from 50.94 Mpa to 34.52 MPa, which was expected. Because graphite experiences very little plastic deformation, the addition of this filler to the IM and 3D printed polymers is attributed to a restrictive effect in the polymer matrices, deforming and restricting their molecular chain movement.[21] There was a decrease

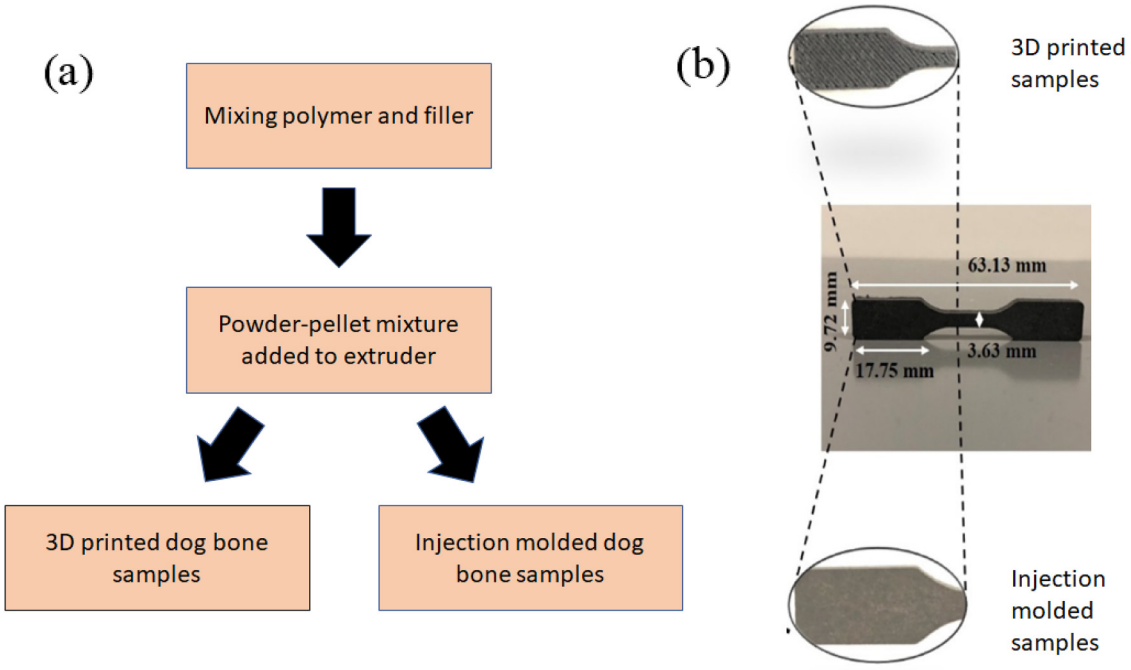

FIG. 1. (a) Process flow used for fabricating 3D-P and IM OMCs. (b) Photograph of an ASTM standard tensile test dog-bone sample fabricated in this work, where the top inset shows the magnified image of the surface revealing a rough surface with 3D-P, compared to the smoother surface for IM.

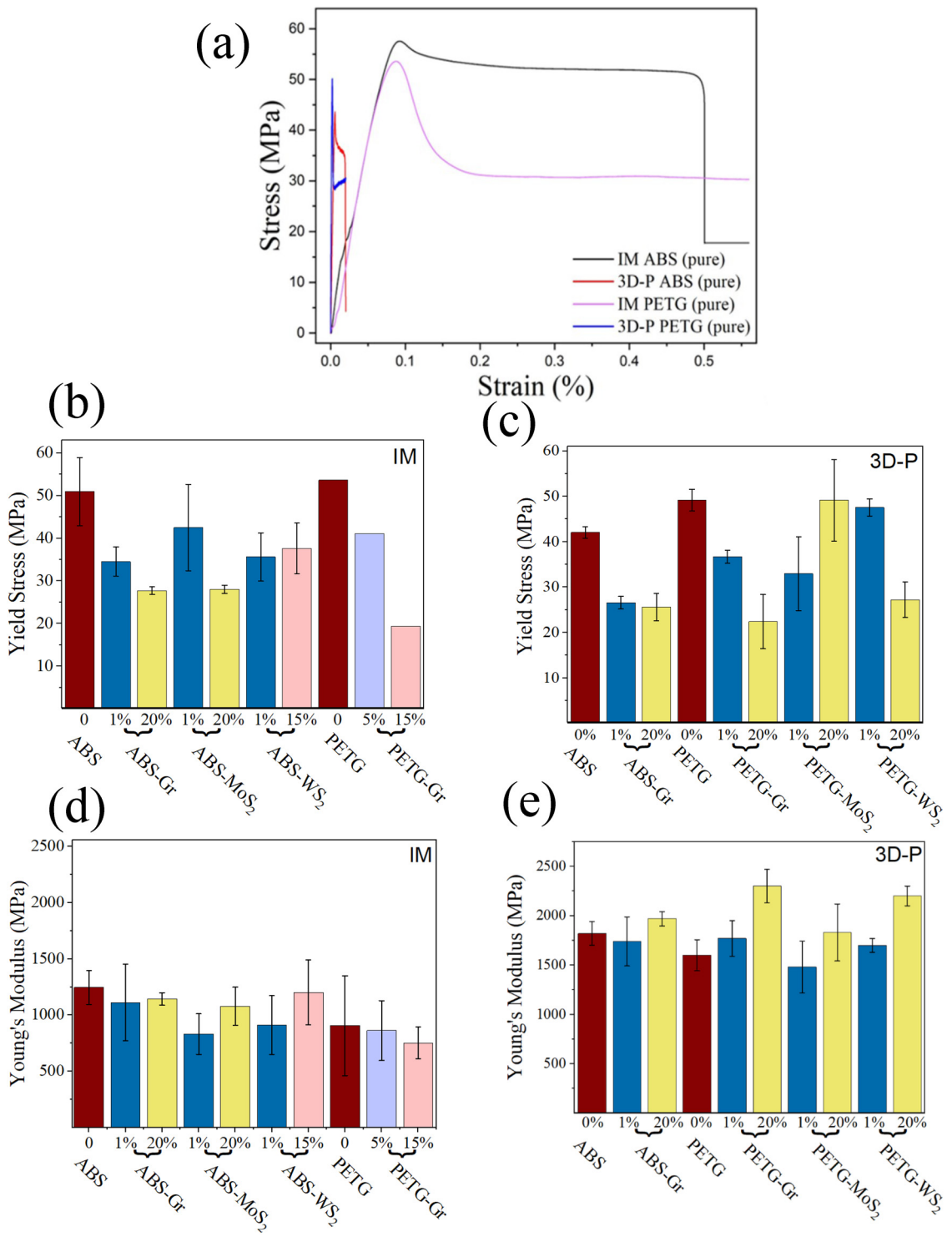

FIG. 2. (a) Stress vs strain curve for injection molded and 3D printed pure (0% loading) ABS and PETG. It can be clearly seen that injection molded samples are more ductile than their 3D printed counterparts. The effect of yield stress on filler concentration is seen in (b) and (c). A general decrement trend is observed in terms of yield stress with increasing filler loading concentration. However, an opposite trend was seen in the case of 3D-P PETG + MoS_2 and WS_2 samples. Young's modulus has been plotted against filler loading concentration in (d) and (e).

in yield stress with the addition of 1% graphite to the 3D-P samples from 49.16 to 36.69 MPa which continued to decrease as the weight percentage increased, as seen by the 15% loaded sample in Fig. 2(b). A similar trend was seen in the cases of MoS_2 infused IM ABS and 3D printed PETG with WS_2. Yield stress followed a decreasing trend with the addition of MoS_2, though WS_2 reacted differently with an initial decrement in yield stress at with 1% weight, but an increase in the yield stress of the PMC at 15% wt. This rise in yield stress at 15% WS_2 concentration is likely related to the mixing inhomogeneity between the filler and the matrix, leading to uneven stress distribution. In such situations, the fillers fail to strengthen the matrix base. Young's modulus shown in the plots of Figs. 2(d) for IM and 3D-P (e), was relatively unchanged in the IM and 3D printed ABS matrix base but in the case of PETG

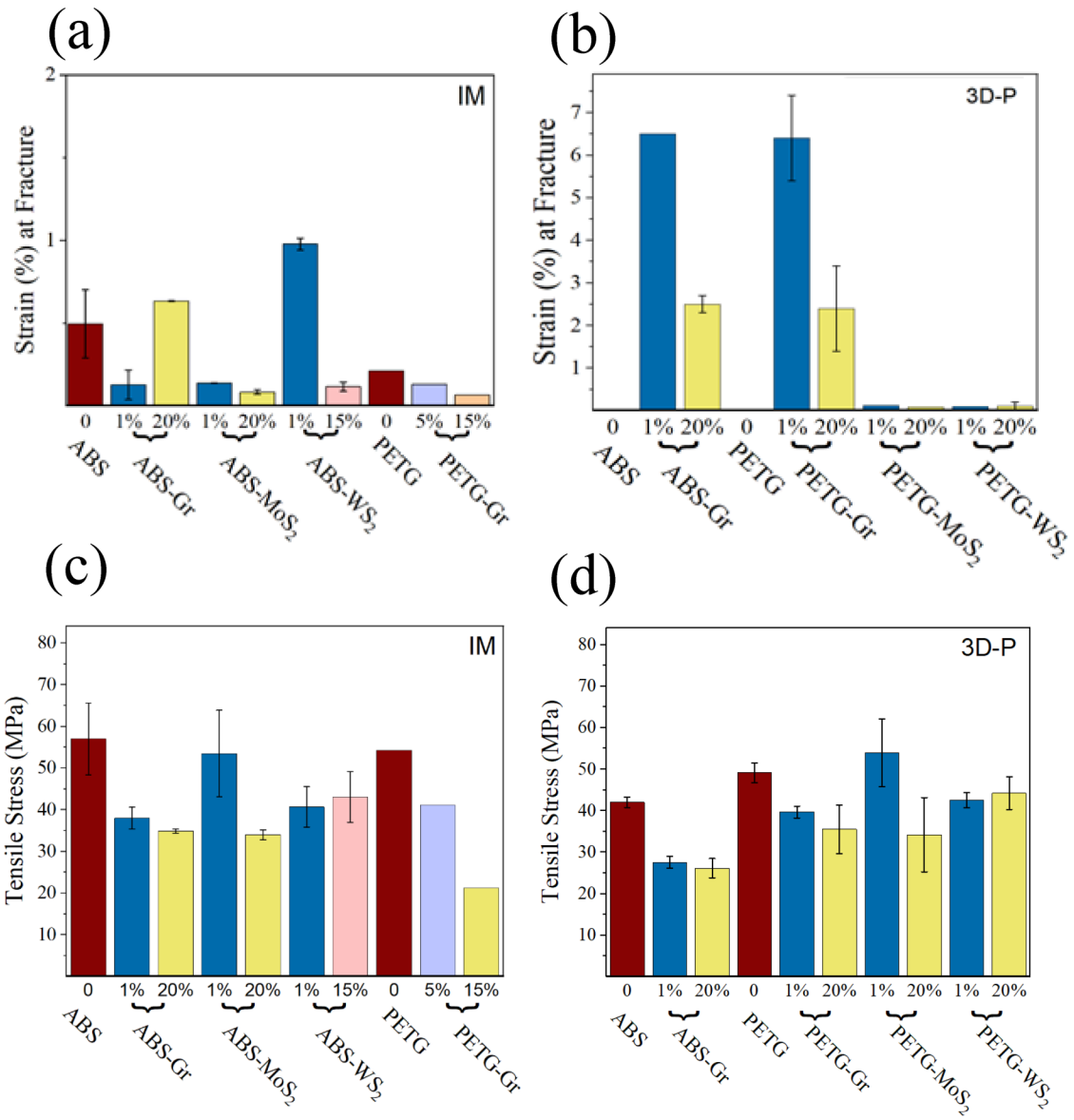

FIG. 3. (a) The strain at fracture for IM and (b) 3D-P ABS and PETG. For both the (c) IM and (d) 3D-P samples, tensile stress was seen to decrease with the addition of filler materials. However, exceptions were noticed in the case of IM ABS and WS_2 samples, where tensile stress was seen to increase at a 15% loading concentration. A similar exception was seen in the case of the 3D-P PETG and WS_2 samples, where tensile stress was seen to decrease first but later increased at higher filler concentration.

with 3D-P, a relatively noticeable increment was noted at 20% loading. Interestingly, similar trends were recorded with MoS_2 and WS_2 infused PMCs in both IM and 3D-P specimens. However, Young's modulus decreased with increasing concentrations of graphite in IM PETG, as is seen from Fig. 2(d), which is likely due to the dispersion inhomogeneity within the IM PETG matrix base.

Figures 3(a) and 3(b) depict the strain (percentage) at fracture for the IM (a) and 3D-P (b) samples. Comparing Figs. 3(a) and 3(b), there is a significant increase of strain (%) at fracture for 3D-P ABS and PETG with graphite fillers. The IM ABS and PETG samples with graphite showed similar trends for strain (%) at fracture, decreasing with an increase of filler concentration. A slight exception was noticed for the ABS specimen; there was an initial decrease with the addition of 1% graphite, but an increase at 20% by weight. Tensile stress seemed to follow a decreasing trend with the increasing filler concentration as shown by the data in Figs. 3(c) and 3(d), with an exception for the case of IM ABS with WS_2 and 3D-P PETG with WS_2. Previously, Hajar *et al.* in 2017 observed a similar decrement in tensile strength with increasing graphite loading in polyethylene oxide (PEO) and polyvinyl chloride (PVC) matrices.[22] Graphite and MoS_2 also showed a decreasing tensile strength with increasing filler content in the 3D-P and IM PMC samples. Tensile stress seemed to follow a decreasing trend with the increasing filler concentration as shown by the data in Figs. 3(c) and 3(d), with an exception for the case of IM ABS with WS_2 and 3D-P PETG with WS_2. Previously, Hajar *et al.* in 2017 observed a similar decrement in tensile strength with increasing graphite loading in polyethylene oxide (PEO) and polyvinyl chloride (PVC) matrices.[22] Graphite and MoS_2 also showed a decreasing tensile strength with increasing filler content in the 3D-P and IM PMC samples.

For the IM samples, the most decrements in yield stress and tensile stress were observed in the PETG-graphite samples. The ABS–WS_2 sample set showed a yield and tensile stress that after an initial decrease at 1% loading, increased significantly with 15% WS_2. For the 3D-P samples, in the ABS–graphite loadings, the yield strength decreased with increasing filler concentrations. Tensile strength also decreased rapidly with the addition of filler at just 1% concentration and continued to decrease marginally with additional concentration (up to 20%). Therefore, a slight deviation in consistency in decrement is recorded. The PETG–graphite samples however, maintained consistency in both tensile strength reduction and increased Young's modulus with increasing filler in the matrices.

C. Fracture surface analysis

After mechanical property analysis, the fractured tensile samples were observed under an optical microscope to examine the distribution of fillers inside the PMCs. A low magnification of 5× zoom was chosen to observe the surface for visual filler dispersion given the large variation in the surface roughness. In general, the 3D-P samples showed better visual dispersion of the filler within

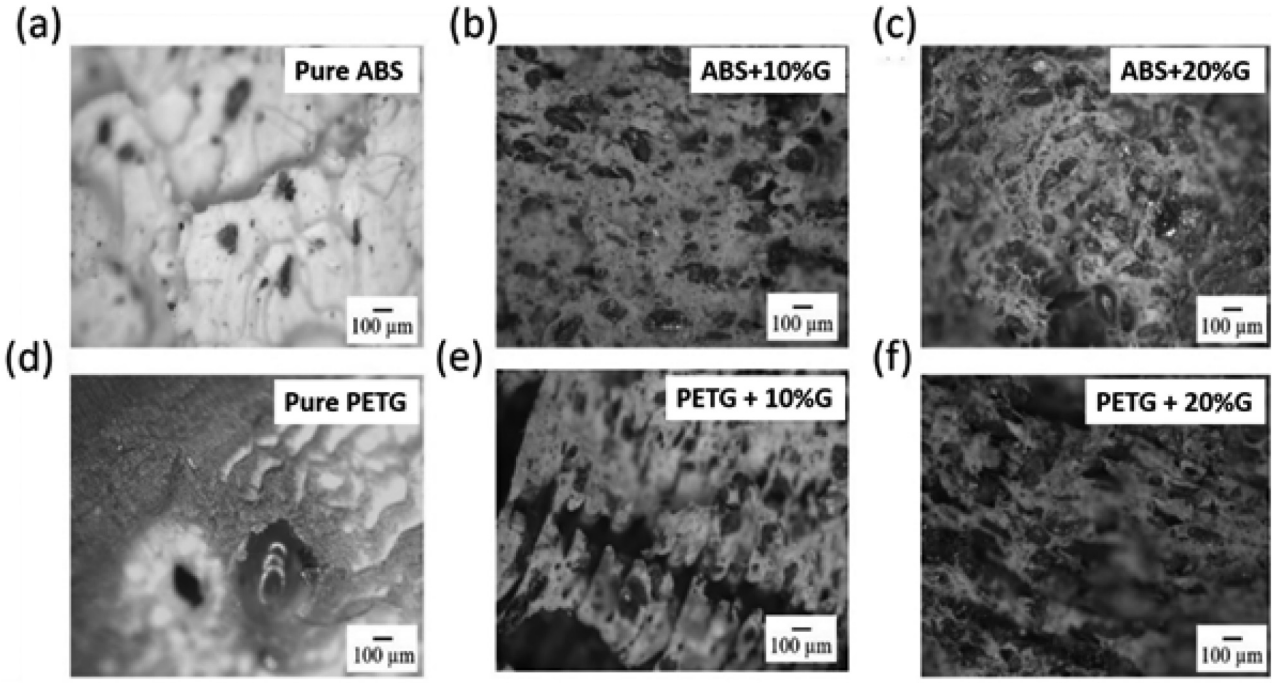

FIG. 4. (a)–(c) show the optical microscopic images of the fractured surface of 3D-P ABS (pure), ABS—10% graphite, and ABS—20% graphite, respectively. (d)–(f) show the 3D-P PETG (pure), PETG—10% graphite and PETG—20% graphite. In both the ABS and PETG samples, large agglomerations of graphite fillers are seen embedded within the matrix phase.

the polymer matrices. Figures 4(a)–4(c) show the fracture surface of 3D-P ABS and graphite samples; ABS (pure), ABS—10% graphite, ABS—20% graphite, respectively. The term "G" in the text labels in Fig. 4 refers to graphite. The fracture surface indicated that the failure in these materials was due to considerable shear forces despite the fact that the stress imposed was purely tensile, a phenomenon best described as resolved shear stress. Comparatively, the 3D printed PETG sample's fracture surfaces are seen in Figs. 4(d)–4(f), stating from Figs. 4(d)–4(f) are 3D printed pure PETG, PETG—10% graphite, PETG—20% graphite, respectively. In comparison to Figs. 4(a)–4(c), fracture surfaces of the 3D-P PETG samples in Figs. 4(d)–4(f) were seen to be rougher and coarser. This because PETG is more ductile than ABS, irrespective of the processing route, confirmed by the mechanical property analysis in Figs. 2 and 3. Identical images were obtained for samples with MoS_2 and WS_2 fillers, where the fillers were seen to exist as chunks within the matrices. The fracture surface images for the IM counterparts were similar but the dispersion of the fillers was more clearly visible in the 3D-P samples.

D. Dynamic friction

Figures 5(a) and 5(b) show the dynamic friction data as a function of filler concentration. The fractured tensile samples (IM and 3D-P) were tested in a ball-pin tribometer to observe the effects of the filler materials (graphite, MoS_2 and WS_2) on frictional properties of the PMCs. Figure 5(c) shows an example of the wear track produced within the PMCs. The reduction in friction using solid lubricants is strongly dependent on the homogeneity and weight percentage of the dispersion phase within the matrix. With greater homogeneity and concentration of the dispersed phase, there is an increased likelihood of reducing shear forces and therefore decreasing friction. The 2D materials often tend to agglomerate at high temperatures, which was observed in this work during IM and 3D-P samples. If these particles agglomerate, they become heavier which decreases their mobility to the surface of the PMC where they are tested for friction and wear. The results suggest that this might be the case for IM ABS with MoS_2 and WS_2. This effect does not limit itself to 2DLMs but is also be observed in 3D materials such as graphite and could be the reason for a sudden rise in dynamic friction at 10% graphite concentration in IM PETG. MoS_2 and WS_2 showed significant friction reduction in the 3D-P PETG samples, as shown in Fig. 5(b). However, graphite being the proven material was seen to successfully reduce dynamic friction in both, IM and 3D printed ABS and PETG.

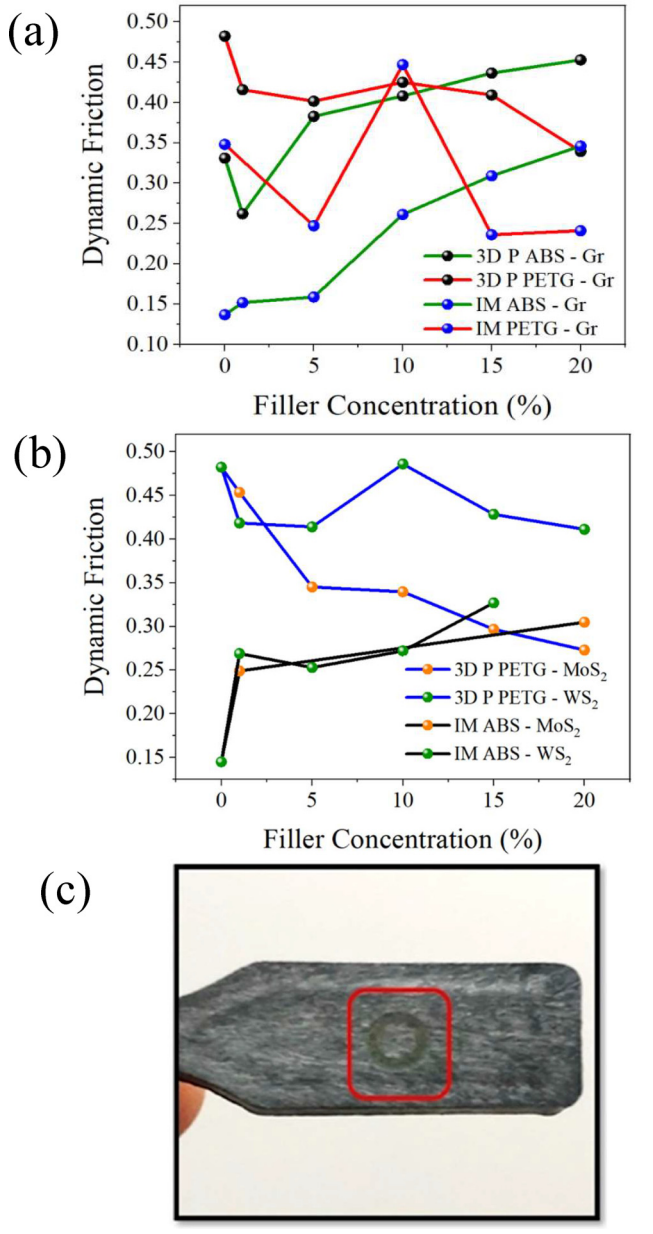

FIG. 5. (a) and (b) exhibit the effect of dynamic friction with filler addition to the matrix base. (a) While graphite being a solid lubricant was able to reduce friction in the case of PETG, an opposite trend is seen in the case of ABS where dynamic friction was seen to increase with increasing filler concentration. The results were similar when MoS_2 and WS_2 were added in the ABS matrix base as shown in (b), while these fillers were able to reduce friction in the PETG samples. (c) The wear track produced by the pin-on disk tribometer for the wear test measurements.

E. Thermal conductivity

In general, ABS and PETG are thermally insulating. However, because graphite is a good thermal conductor and MoS_2/WS_2 are semiconductors, the PMCs were tested for thermal conductivity to see if the conductive fillers were able to influence the thermal conductivity of the insulating matrix bases. The thermal conductivity of the samples was measured using the Hot Disk 2400 Source at room temperature. Figures 6(a)–6(d) show the thermal conductivity as a function of the filler concentration where the thermal conductivity increased as the filler concentration increased. For graphite incorporated in IM and 3D-P ABS samples, the 3D-P ABS–graphite showed better conductivity [Fig. 6(a)]. A similar trend was also observed in Fig. 6(b) for graphite–PETG samples, where thermal conduction was better in 3D-P samples compared to their IM counterparts. In Figs. 6(c) and 6(d), MoS_2 was seen to

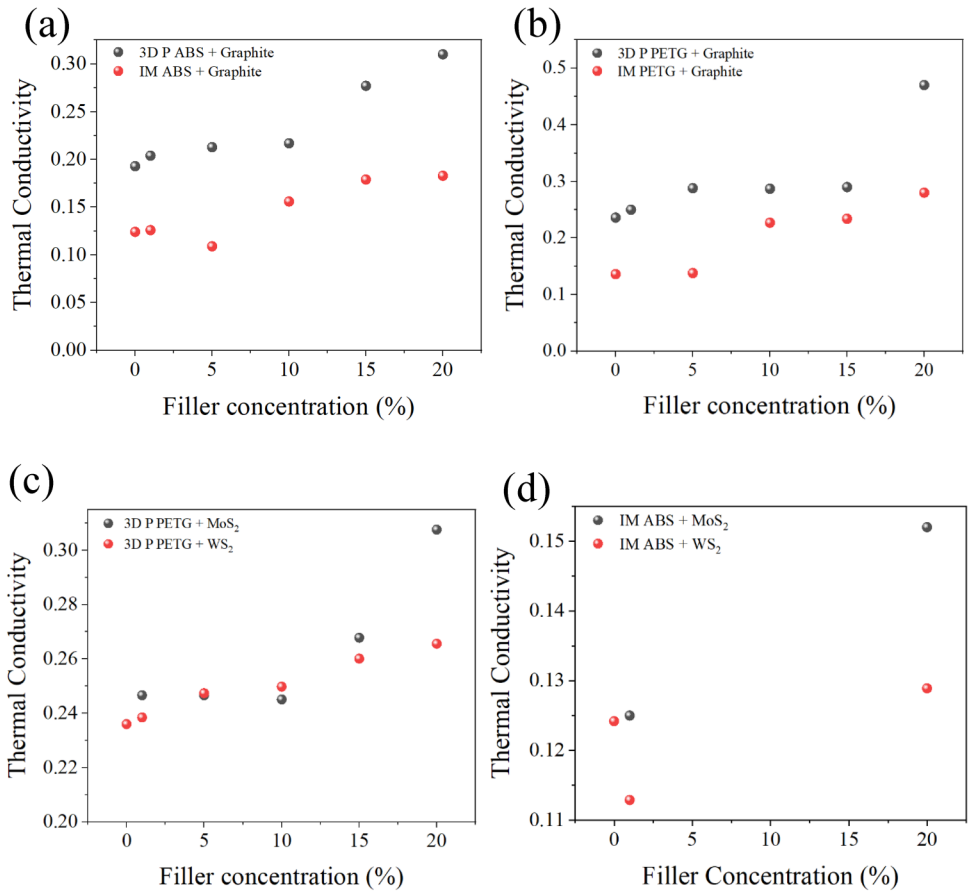

FIG. 6. Shows the effect of thermal conductivity up on increasing filler concentration in IM and 3D-P ABS and PETG samples. Graphite being conductive, helps in increasing thermal conductivity in both the ABS and PETG samples irrespective of their processing route. This can be clearly seen in (a) and (b); (c) and (d) exhibit the same behavior for MoS_2 and WS_2 fillers.

have a more definite effect in terms of thermal conductivity enhancement compared to WS_2, in both 3D-P PETG and IM ABS samples. Heat conduction is expected to substantially improve with increasing filler concentration beyond the 20% maximum studied here, since the filler material properties will dominate at the higher loadings to influence the thermal properties.

III. CONCLUDING REMARKS

In this study, the mechanical, frictional, and thermal properties of IM and 3D-P ABS and PETG matrix infused with the filler materials, such as graphite, MoS_2 and WS_2, was investigated. A slightly similar work was reported by Bermudez and her colleagues who added MoS_2 and two thermotropic liquid crystals to Polyamide 6 and determined friction and wear using a pin-on-disk tribometer.[23] Upon increasing concentration of filler materials, the tensile strength and the yield strength of the PMCs decreased—except for samples containing WS_2. The WS_2 infused ABS and PETG samples show an increase in both these tensile parameters. The PETG–graphite samples processed by both IM and 3D-P display the most consistent response to an increase in filler concentration. Graphite—a prototypical solid phase lubricant—also successfully reduces friction in the PETG PMCs with increasing concentration, similarly to MoS_2 and WS_2. Thermal conductivity increases in ABS and PETG samples irrespective of their processing routes with the addition of filler material. While graphite is a conductor while MoS_2 and WS_2 are semiconductors, in all three cases the thermal conductivity in the insulative ABS and PETG was seen to increase with filler loading. While our work explored graphite as one of the filler materials, it will be interesting to extend this analysis to graphene oxide (GOx) as the filler material for a future study, given the interesting properties of GOx, to potentially further improve the performance of the composites.[24]

AUTHORS' CONTRIBUTIONS

G.G., S.M., and N.H. contributed equally to this work.

ACKNOWLEDGMENTS

The authors greatly appreciate support received from the Army Research Office (Grant No. W911NF-15-1-0425) that enabled them to pursue this work. G.G. acknowledges useful discussions and assistance provided by Kishan Jayanand in the Nanoscale Materials and Devices Laboratory at UNT. A.B.K. also acknowledges support received from the UNT PACCAR Endowed Professorship and Institute support.

REFERENCES

[1]G. A. Ozin and A. C. Arsenault, *Nanochemistry: A Chemical Approach to Nanomaterials*, 1st ed. (RSC Publishing, London, 2005), ISBN: 13: 978-0854046645.
[2]X. Duan, C. Wang, A. Pan, R. Yu, and X. Duan, Chem. Soc. Rev. **44**, 8859 (2015).
[3]J. A. Desai, N. Adhikari, and A. B. Kaul, RSC Adv. **9**, 25805 (2019).
[4]S. K. Mahatha, K. D. Patel, and K. S. R. Menon, J. Phys. Condens. Mater. **24**, 475504 (2012).
[5]W. Zhao, Z. Ghorannevis, L. Chu, M. Toh, C. Kloc, P.-H. Tan, and G. Eda, ACS Nano **7**, 791 (2013).
[6]A. Pakdel, C. Zhi, Y. Bando, and D. Goldberg, Mater. Today **15**, 256 (2012).
[7]A. B. Kaul, J. Mater. Res. **29**, 348 (2014).
[8]S. Chugh, N. Adhikari, J. H. Lee, D. Berman, L. Echegoyen, and A. B. Kaul, ACS Appl. Mater. Interfaces **11**, 24349 (2019).
[9]J. Ma, H. Bai, W. Zhao, Y. Yuan, and K. Zhang, Sol. Energy **160**, 76 (2018).
[10]A. S. Bandyopadhyay, N. Adhikari, and A. B. Kaul, Chem. Mater. **31**, 9861 (2019).
[11]X. Li, Y. Gao, J. Xing, Y. Wang, and L. Fang, Wear **257**, 279 (2004).
[12]M. Y. Cho, J. Ju, S. J. Kim, and H. Jang, Wear **260**, 855 (2006).
[13]S. Mazumder, J. A. Catalan, A. Delgado, H. Yamaguchi, C. N. Villarubia, A. D. Mohite, and A. B. Kaul, Compos. Sci. Technol. **182**, 107697 (2019).
[14]X. Zhao, Q. Zhang, D. Chen, and P. Lum, Macromolecules **43**, 2357 (2010).
[15]T. Kuilla, S. Bhadra, D. Yao, N. H. Kim, S. Bose, and J. H. Lee, Prog. Polym. Sci. **35**, 1350 (2010).
[16]J. N. Coleman, U. Khan, W. J. Blau, and Y. K. Gunko, Carbon **44**, 1624 (2006).
[17]B. P. Singh, B. K. Jena, S. Bhattacharjee, and L. Besra, Surf. Coat. Technol. **232**, 475 (2013).
[18]B. Wetzel, F. Haupert, K. Friedrich, M. Q. Zhang, and M. Z. Rong, Polym. Eng. Sci. **42**, 1863 (2007).
[19]D. M. Bigg, Polym. Eng. Sci. **19**, 1188 (1979).
[20]Z. Spitalsky, D. Tasis, K. Papagelis, and C. Galiotis, Prog. Polym. Sci. **35**, 357 (2010).
[21]C. Morrison, M. Zhang, and A. Jikov, Procedia Mater. Sci. **3**, 1848 (2014).
[22]C. Wang, Z. X. Guo, S. Fu, W. Wu, and D. Zhu, Prog. Polym. Sci. **29**, 1079 (2004).
[23]M. D. Bermudez, F. J. Carrion-Vilches, I. Martinez-Mateo, and G. Martinez-Nicolais, J. Appl. Polym. Sci. **81**, 2426 (2001).
[24]I. Moon, J. Kim, and H. Lee, Sci. Rep. **3**, 1112 (2013).
[25]See supplementary material at https://doi.org/10.1116/6.0000121 for detailed tensile test plots for the ABS and PETG composites.